
This manuscript is a preprint and was submitted for publication in *Geophysical Research Letters* in January 2021. **Please note that this manuscript has not undergone formal peer review, nor has it been formally accepted for publication.** Subsequent versions of this manuscript may have slightly different content. Please feel free to contact Oliver Lamb with your feedback or comments using the email address below.

Acoustics from low-magnitude fluid-induced earthquakes in Finland

Oliver D. Lamb[1], Jonathan M. Lees[1], Peter E. Malin[2,3], Tero Saarno[4]

[1]Department of Geological Sciences, University of North Carolina at Chapel Hill, Chapel Hill, NC, USA
[2]Earth and Ocean Sciences, Nicholas School of the Environment, Duke University, Durham, NC, USA
[3]ASIR Advanced Seismic Instrumentation and Research, Dallas, TX, USA
[4]St1 Deep Heat Oy, Helsinki, Finland

Key Points:

- Audible noises were reported during induced earthquake sequence in Helsinki Metropolitan area in 2018
- Two microphone arrays were deployed and captured signals from 39 earthquakes with moment magnitudes ranging from -0.07 to 1.87.
- Acoustics were likely generated by ground reverberation during the arrival of seismic body waves at the surface.

Corresponding author: Oliver Lamb, `olamb@email.unc.edu`

Abstract

Earthquakes are frequently accompanied by public reports of audible low-frequency noises. In 2018, public reports of booms or thunder-like noises were linked to induced earthquakes during a Engineered Geothermal System project in the Helsinki Metropolitan area. In response, two microphone arrays were deployed to study these acoustics while stimulation at the drill site continued. During the 11 day deployment, we find 39 earthquakes accompanied by recognizable atmospheric acoustics. Moment magnitudes of these events ranged from -0.07 to 1.87 with located depths of 4.8 to 6.5 km. Analysis of the largest event revealed a broadband frequency content, including in the audible range, and high apparent velocities across the arrays. We conclude that the audible noises were generated by local ground reverberation during the arrival of seismic body waves. The inclusion of acoustic monitoring at future geothermal development projects will be beneficial for studying seismic-to-acoustic coupling during sequences of induced earthquakes.

Plain Language Summary

Earthquakes are often accompanied by low thunder-like or booming noises. This was the case during geothermal pilot project in the Helsinki Metropolitan area in the summer of 2018, where dozens of local residents reported noises while small earthquakes were occurring below. To investigate how these noises might be generated, we deployed two clusters of microphones in the area to record the noises. Over 11 days, we found 39 earthquakes that also generated noises loud enough to be recorded by the microphones. The timing of noises arriving at each cluster of sensors led us to conclude that these noises were being generated by shaking of the ground around the microphones. This incident demonstrated how noises from induced earthquakes might generate major public concern and that future geothermal projects can benefit from deploying microphones to help with their response.

1 Introduction

Earthquakes of a wide range of magnitudes are commonly accompanied by reports and/or measurements of atmospheric acoustic waves at various epicentral distances. These waves may have frequencies ranging from infrasonic (<20 Hz) up to and beyond the minimum limit of human hearing ability (20 - 70 Hz). Cases of the latter have been described as low rumbling sounds or booms (Michael, 2019), and have been reported for shallow (<2 km) earthquakes in the USA (Ebel et al., 1982) and France (Sylvander & Mogos, 2005; Sylvander et al., 2007; Thouvenot et al., 2009). The event magnitudes associated with these sounds have been stated to be as low as -2 and -0.7, respectively. Audible noises are also frequently reported for larger magnitude earthquakes, and accompanied by the frequent detection of infrasonic acoustic waves at global distances (e.g. Mikumo, 1968; Young & Greene, 1982; Olson et al., 2003; Le Pichon et al., 2003; Mutschlecner & Whitaker, 2005; Le Pichon et al., 2006; Arrowsmith et al., 2012). Mapping of acoustic sources during and immediately after earthquakes has identified three sources of earthquake acoustics (Arrowsmith et al., 2010): i) 'epicentral' (i.e. seismic-to-acoustic coupling directly above or near the earthquake epicenter; Mikumo, 1968; Young & Greene, 1982), ii) 'local' (i.e. generated by the passage of seismic waves near sensor located at distance from epicenter; Cook, 1971; Kim et al., 2004) and iii) 'secondary' (i.e. generated by interaction of seismic waves with topographic features; Young & Greene, 1982; Mutschlecner & Whitaker, 2005; Shani-Kadmiel et al., 2018; Johnson et al., 2020). 'Epicentral' acoustics have been attributed primarily to vertically propagating body waves (particularly P- and SV-waves) coupling directly into the atmosphere through ground motion at the Earth's surface (Hill et al., 1976). Seismo-acoustic recordings of earthquake acoustics at local or epicentral distances are limited to only a few studies (e.g. Hill et al., 1976; Sylvander et al., 2007; Johnson et al., 2020). Here we describe a case study of epicentral acoustic waves generated by earthquakes during a hydraulic stimulation project in Finland, one of the first documented recordings of acoustics from an induced earthquake sequence and are amongst the lowest magnitude events to be recorded.

2 St1 Deep Heat Oy Venture

The St1 Deep Heat Oy energy-company Engineered Geothermal System (EGS) pilot project was located in the Helsinki Metropolitan area within the campus of Aalto University (Fig. 1). The aim of the project was to develop an EGS facility in order to produce a sustainable baseload for the local district heating system (Kwiatek et al., 2019). In 2018, a 6.1 km deep stimulation well was drilled into crystalline Precambrian Svecofennian basement rocks consisting of granites, pegmatites, gneisses, and amphibolites (Kwiatek et al., 2019); this bedrock is only locally covered by a thin (<10 m) layer of glacial till or soil (Hillers et al., 2020). From 4 June to 22 July 2018, a total of 18,160 m^3 of water was pumped into the stimulation well at depths of 5.7 to 6.1 km; this included moving injection intervals and multiple stoppages for a few days (Kwiatek et al., 2019; Hillers et al., 2020). Induced seismicity was monitored by an extensive seismic network, including 3-component borehole seismometers installed in 0.3 to 1.15 km deep wells at distances up to 8.2 km from the drill site (Fig. 1). The purpose of the seismic network was to provide accurate hypocenter locations and magnitudes of induced earthquakes for both industrial and regulatory purposes (i.e. Traffic Light System; Kwiatek et al., 2019; Ader et al., 2020).

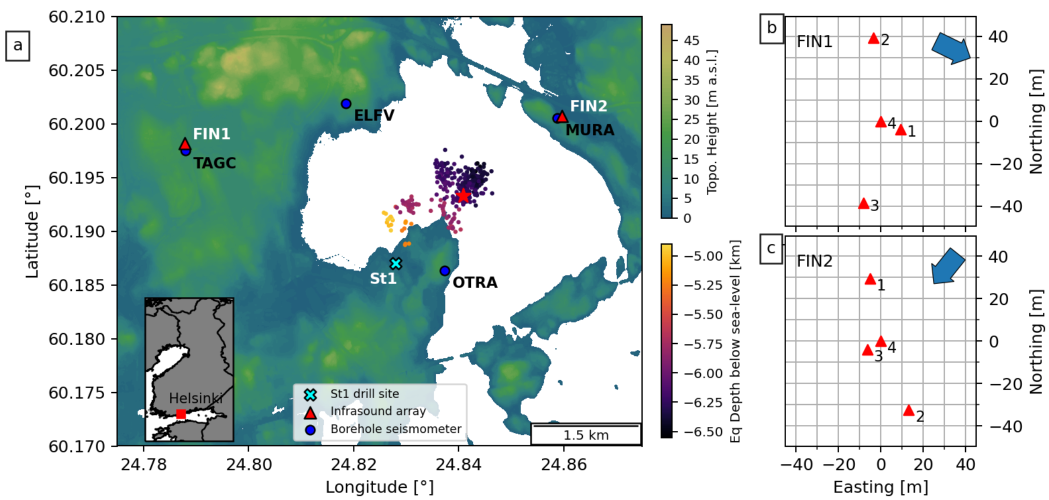

Figure 1. (a) Topographic map of the region around the St1 drill site (cyan cross) showing locations and names of borehole seismic stations (blue circles) and temporary acoustic arrays (red triangles). Also plotted are locations of earthquakes recorded during the acoustic deployment, colored by depth. Red star indicates the location of the M_w 1.87 event. Inset: Map of Finland showing location of the Helsinki Metropolitan area. Panels (b) and (c) show the infrasound sensor distribution for arrays FIN1 and FIN2, respectively, with back azimuth direction to the ST1 drill site indicated by the blue arrow.

From 4 June to 1 August 2018, a total of 8412 earthquakes were automatically recorded by the network out of which 1977 were suitable for relocations and magnitude calculations (Kwiatek et al., 2019). These events were located across three distinct clusters ranging in depths of 4.8 – 6.6 km and moment magnitudes (M_w) of -0.76 to 1.86 (Fig. S1 in

Supporting Information). Fault plane solutions for a set of selected events indicated reverse faulting along pre-existing fractures associated with NW-SE trending fault zones reactivated by the hydraulic injection (Hillers et al., 2020). The Institute of Seismology at the University of Helsinki (ISUH) collected 220 public reports of felt earthquakes, which unexpectedly also included dozens of audible disturbances, typically described as thunder- or blast-like (Ader et al., 2020; Hillers et al., 2020). The largest and most reported event was a M_w 1.87 event on 8 July 2018 located at 6.3 km depth (Fig. 1). This event generated 78 public reports and was apparently heard up to 9 km away from the epicenter (Hillers et al., 2020). Notably, spatial distributions of the reports were strongly correlated with the SH radiation pattern of the reverse faulting mechanism in the event (Hillers et al., 2020).

3 Data and Methods

In response to the reports of audible earthquake events, we deployed two temporary arrays of infrasound microphones in the area from 7 – 18 July to study the nature of these atmospheric acoustics. The arrays were deployed at distances of ~2.5 and ~2.2 km from the St1 drill site. Each deployment consisted of three microphones extended on cables up to 35 m from a central data recorder, where a fourth microphone was located (Fig. 1b, c). The data recorder was a REFTEK RT 130 data logger which provided a 24-bit, GPS-time synchronized recording set to 100 samples per second, resulting in an anti-aliasing Finite Impulse Response (FIR) filter cut off of 40 Hz. The microphones were identical infraBSU (vers1) microphones, which incorporate a MEMS sensor and capillary filters to provide a flat response at >0.1 Hz (Marcillo et al., 2012). To aid analysis and interpretation of acoustic data in this study, we also included seismic data from borehole seismometers located near each array (TAGC and MURA; Fig. 1a). Each seismometer was composed of a three-component Sunfull PSH geophone sensor (f_N = 4.5 Hz) recording at 500 samples per second and located ~1.15 km below the surface (For more information, see Kwiatek et al., 2019).

For this study, all data were filtered with a 2 Hz high-pass Butterworth filter to reduce continuous background noise (unless otherwise indicated). Data were manually inspected for consistent arrivals across at least two microphones in each array to assess if earthquake-generated atmospheric acoustic waves were detected following an induced earthquake. To estimate the arrival times for different body wave phases at each array, we use P- and S-wave velocities of 6.25 and 3.75 km.s^{-1} respectively, as estimated from borehole logs at the St1 drill site (see supplementary materials in Kwiatek et al., 2019). One of the key advantages of deploying acoustic microphones in an array configuration is it permits the calculation of back azimuth direction and slowness of acoustic waves propagating across the deployment. Here we estimated back azimuths and slowness values for 0.1 s windows with 90% overlap within the first 3 s after the initiation time of the earthquake. We used waveform envelopes, determined from the square root of the Hilbert Transform, which were then smoothed using the average of an 8 sample moving window (Fig. 4a, b). All analysis presented here was carried out within the ObsPy python package (Krischer et al., 2015).

4 Observations

During 7 – 18 July, 266 earthquakes were detected and relocated within a few hundred metres of the stimulation interval. These events occurred at depths of 4.8 to 6.5 km below sea level and had moment magnitudes ranging from -0.19 to 1.87 (Fig. 1a, 2a, b). Of the 266 earthquakes, 39 were followed shortly by atmospheric disturbances across at least one array that may be interpreted as earthquake associated acoustic waves (Fig. 2). Atmospheric disturbances were more commonly seen at FIN2 (n=36) than FIN1 (n=9), with only 3 events seen exclusively at the latter. The smallest event was a M_w -0.07 on

8 July, and the largest was the widely heard M_w 1.87 on the same day (Fig. 2c). As the latter earthquake produced the highest signal-to-noise ratios at both microphone arrays, the remainder of this section will focus on the analysis of acoustic data from this particular event.

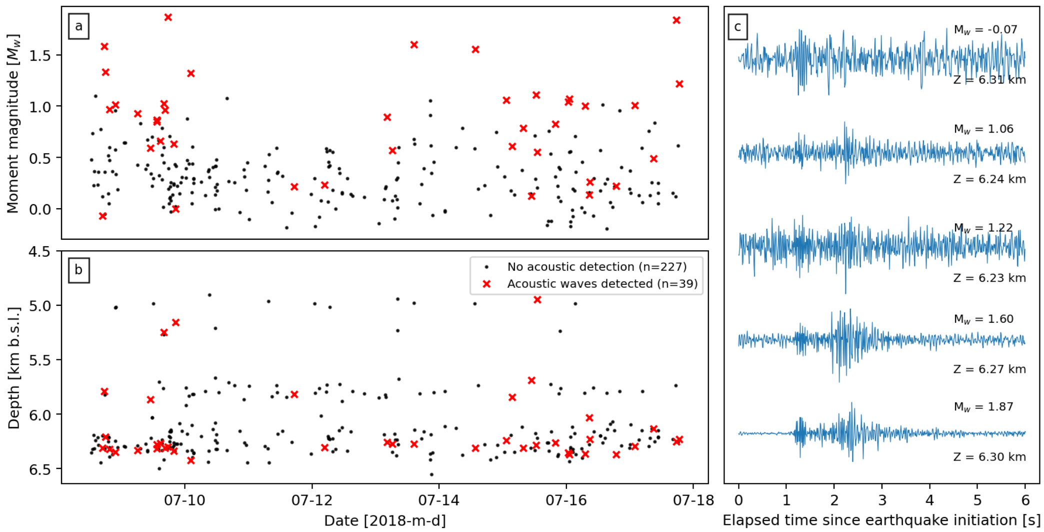

Figure 2. Moment magnitudes (a) and depths (b) of the 266 relocated seismic events recorded during the infrasound array deployment near the St1 Deep Heat Oy EGS project. Red ‘x’ indicate the events which were detected by at least one acoustic array. (c) 6 s of normalised acoustic data (highpass filtered at 5 Hz) recorded by sensor 2 at FIN2 after the initiation of five example earthquakes, including the lowest and highest magnitude events. Calculated M_w and depth (Z) of each event is indicated on the right. (See figures S2 to S11 in Supporting Information for waveforms and frequency spectrograms from all microphones for each event.)

For the M_w 1.87 event the acoustic data recorded at FIN2 have peak amplitudes an order of magnitude larger than those recorded at FIN1 (Fig. 3c, g). Frequency spectra highlight the broadband nature of the atmospheric acoustics, with frequencies ranging from 2 to 50 Hz (Fig. 3d, h). The acoustic waves and their spectra at each array appear to show distinct multi-phase arrivals that correlate with seismic waves recorded at the nearby borehole seismometers (Fig. 3a, b, e, f). The different arrival phases at each array appear to be coincident with the predicted arrivals of P- and S-waves (dotted and dashed red lines in Fig. 3). The highest acoustic amplitudes are correlated with the arrival of the S-waves at each array. Calculated values of back azimuth and slowness are generally well scattered across the analysed 3 s time window (Fig. 4b-d). However, at or near the estimated time of arrivals for P- and S-waves (red lines in Fig. 4a, b), the back azimuths indicate arrivals from the direction of the M_w 1.87 event epicenter (Fig. 4c, d). Slowness values at these times indicate relatively high propagation velocities across the array (Fig. 4e, f).

5 Discussion

Here we have presented evidence for infrasonic and audible atmospheric acoustics generated by low magnitude fluid-induced earthquakes. These observations are notable for two reasons: i) these are the first recorded earthquake-generated acoustics from induced earthquakes, and ii) they represent the lowest magnitude events to be recorded

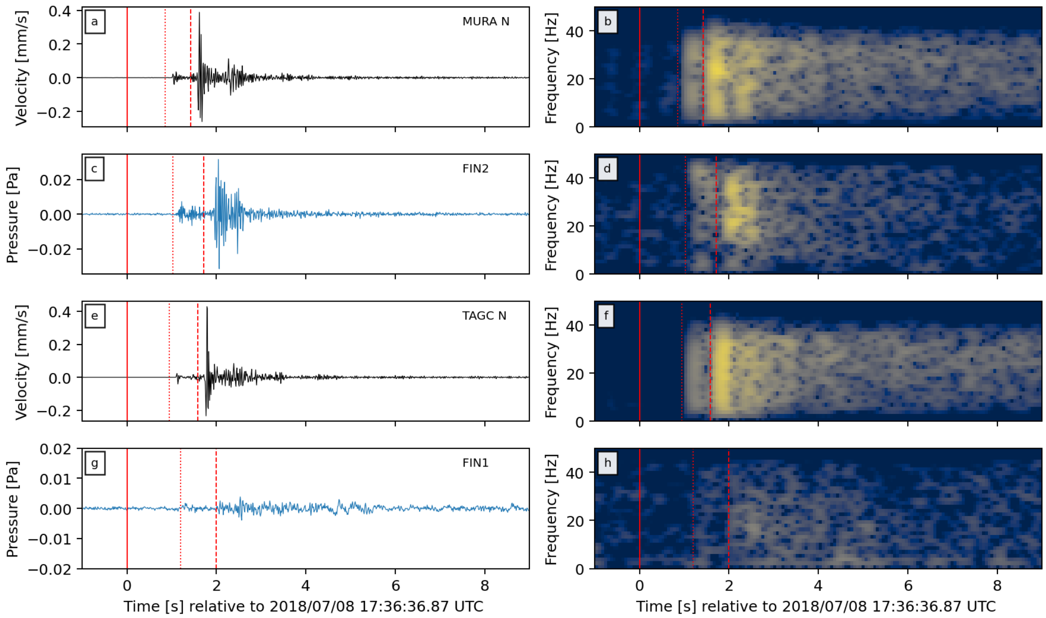

Figure 3. Waveforms (left column) and their respective frequency spectrograms (right column) of the M_w1.86 event as recorded by seismic station MURA (a, b), acoustic array FIN2 (c,d), seismic station TAGC (e, f) and acoustic array FIN1 (g, h). Note that the seismic waveforms are from the north component of the station. Also plotted is the time of the event (solid red line), as well as predicted arrival times for P- and S-wave phases (dotted and dashed red lines, respectively).

by acoustic microphones. (There are reports of audible noises from earthquakes with magnitudes as low as -2 (Thouvenot et al., 2009) but these events were not recorded with microphones.) Manual inspection of acoustic data identified at least 39 events where acoustic waves were recorded propagating across at least one array of sensors (Fig. 2). This represents only 15% of all earthquakes relocated during the deployment, but the location of the arrays within a large metropolitan area with a large number of noise sources may have acted to reduce this proportion. The acoustic waves contained broadband frequency ranges from 2 up to 40 Hz, and possibly higher but is limited by the anti-alias FIR filter of the sample recording rate (Fig. 3d, h). This frequency range overlaps with the lower range of human hearing (down to 20 Hz), therefore confirming that thunder- or blast-like sounds heard by the public were generated by the earthquakes (Ader et al., 2020; Hillers et al., 2020). These frequency ranges also match previously reported values from audible natural earthquakes (Hill et al., 1976; Sylvander et al., 2007).

The significant scattering of back azimuth and slowness values before the arrival of atmospheric acoustics (Fig. 4) is interpreted to be a result of the large number of noise sources found in a metropolitan area. However, during the expected arrival of the P- and S-waves the back azimuth values align at or around the direction of the earthquake epicenter (Fig. 4c, d). Simultaneously, the slowness values indicate relatively high propagation values across the array (Fig. 4e, f). These values correlate with waves of either high velocities (>1 kms^{-1}) or near-vertical wave arrival directions at the array. Considering the ratio between earthquake depths (4.8 – 6.5 km) and epicenter-array distances (<2.5 km), it is reasonable to expect near vertical arrival angles of seismic waves at each array. Therefore, the atmospheric acoustics recorded during the largest earthquake, and all other recorded events, were generated by ground motion during and immediately af-

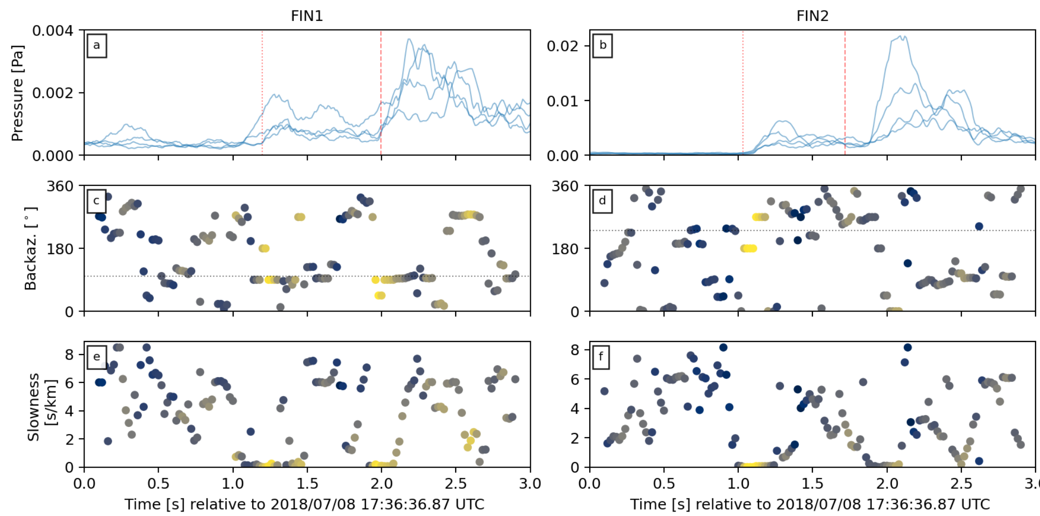

Figure 4. Beamforming results for arrays FIN1 (left column) and FIN2 (right column) for the first 3 seconds after the M_w1.86 event. (a, b) Smoothed waveform envelopes from each element in each array. Dotted and dashed lines plot the estimated arrival times of P- and S-waves, respectively. (c, d) Back azimuth calculations for 0.2 s moving windows with 90% overlap. Horizontal dotted lines plot the azimuth from each array to the M_w1.86 event epicenter. (e, f) Calculated slowness values across each array for each 0.2 s window. Points in panels c-f are colored by relative power, where lighter colors indicate higher relative power (i.e. the signal power of the mean waveform for peak slowness divided by average element power in same time window).

ter the arrival of P- and S-waves at the ground surface within close proximity of the microphone arrays.

A notable observation from the public reports compiled during the induced earthquake sequence is the geographical distribution of disturbances correlated with the radiation patterns of S-waves (See Fig. 5 in Hillers et al., 2020). The FIN2 acoustic array was located adjacent to the area with the greatest number of reports. This pattern correlates with the amplitude difference between the acoustic waves recorded at FIN1 and FIN2 for the M_w 1.86 event, with amplitudes an order of magnitude higher at the latter than the former (Fig. 3c, d). Furthermore, a higher number of earthquake-generated acoustic waves were recorded at FIN2 (N=36) than at FIN1 (N=9). Another factor to consider is that the FIN1 array was deployed on the margin of an active golf course which was built on top of a former municipal waste landfill, while FIN2 was deployed in an area where buildings are frequently constructed directly onto outcropping bedrock. This suggests that the presence of a soft sedimentary layer above the bedrock may act as a dampener during seismic-to-acoustic coupling.

Given that the infrasound sensors are typically placed in direct contact with the ground surface during deployments, contamination of recorded infrasound signals by physical shaking of the sensor could be a concern. However, testing of the seismic response of various acoustic sensors have consistently concluded that physical vibration does not significantly influence the recorded infrasound signals (Bedard, 1971; Hill et al., 1976; Sylvander et al., 2007). The MEMS-based microphones used in this study (InfraBSU vers1) have low inertial mass and are similar in design to the MEMS-based transducers described in Marcillo et al. (2012). These sensors were found to have minimal seismic-to-noise coupling during calibration studies at the Facility for Acceptance, Calibration and Testing site at the Los Alamos National Laboratory (Johnson et al., 2020). Therefore, we do not consider direct seismic shaking of the sensor to be of importance in the acoustic signals presented here.

A common observation in previous earthquake acoustic studies is the presence of secondary infrasound generated away from the earthquake epicenter (Young & Greene, 1982; Le Pichon et al., 2003; Mutschlecner & Whitaker, 2005; Arrowsmith et al., 2010; Shani-Kadmiel et al., 2018; Johnson et al., 2020). These acoustics are confirmed to be caused by the interaction of surface waves with topography or other significant crustal features such as sedimentary basins (Mutschlecner & Whitaker, 2005; Arrowsmith et al., 2010). These are usually manifested as a unusually long coda of secondary arrivals after the local infrasound phases (e.g. Johnson et al., 2020). The infrasound waves described here have relatively short durations with no significant coda, therefore we infer that no secondary infrasound has been generated by the induced earthquakes. We interpret this as a result of the low magnitudes of the events, as well as the lack of steep topographical features around the St1 drill site (Fig. 1a). However, due to the location within an metropolitan area, we cannot rule out the presence of acoustics generated by mechanical shaking of buildings or other structures (e.g. bridges) near each array. Altogether, we interpret the acoustics presented here as 'epicentral' earthquake acoustics generated by ground surface reverberation during the direct arrival of body waves generated by fluid-induced earthquakes.

6 Conclusions

Acoustic monitoring can help explain human observations and may also provide quantitative insights into the mechanics of ground motions responsible for generating earthquake sounds. Here we have presented acoustic events recorded within the Helsinki Metropolitan area in July 2018 during hydraulic stimulation at a pilot Engineered Geothermal System project. Based on the estimated timing of body wave arrivals, frequency content of the waveforms, as well as estimated slowness calculations, we have interpreted these acoustic events as being generated by reverberation of the ground surface during the arrival of P- and S-waves from induced low magnitude earthquakes. Although only a minor proportion of induced earthquakes generated recognizable acoustic waves, events with moment magnitudes ranging from -0.07 to 1.87 were recorded with acoustic microphones at the surface. As far as we are aware, these events represent the first induced earthquakes and are amongst the lowest magnitude events to be recorded with acoustic microphones. Given that Traffic Light Systems are increasingly being implemented to reduce the potential seismic hazard due to induced seismicity (Ader et al., 2020), and the considerable public interest generated by audible earthquakes in the Helsinki Metropolitan area (Ader et al., 2020; Hillers et al., 2020), future projects for developing geothermal systems can benefit from deploying acoustic sensors to provide more detailed information in responses to public concern.

Acknowledgments

The authors wish to thank Dr Peter Leary and the technicians at the St1 Deep Heat project for their help and logistical support during the acoustic sensor deployment. This research was performed while ODL held an NRC Research Associateship with the U.S. Army Research Laboratory/Army Research Office while based at the University of North Carolina at Chapel Hill. All acoustic data presented here will be made available, without undue reservation, to any qualified researcher. Data from the borehole seismometers were transmitted to the Institute of Seismology at the University of Helsinki as part of a regulatory agreement with the city of Espoo and have not been released to the public. Topographic data used in Fig. 1a were downloaded from the National Land Survey of Finland via the Open data file download service (last accessed December 2020).

References

Ader, T., Chendorain, M., Free, M., Saarno, T., Heikkinen, P., Malin, P. E., … et al. (2020). Design and implementation of a traffic light system for deep geothermal well stimulation in Finland. *Journal of Seismology*, *24*(5), 991–1014. doi: 10.1007/s10950-019-09853-y

Arrowsmith, S. J., Burlacu, R., Pankow, K., Stump, B., Stead, R., Whitaker, R., & Hayward, C. (2012). A seismoacoustic study of the 2011 January 3 Circleville earthquake. *Geophysical Journal International*, *189*(2), 1148–1158. doi: 10.1111/j.1365-246X.2012.05420.x

Arrowsmith, S. J., Johnson, J. B., Drob, D. P., & Hedlin, M. A. (2010). The seismoacoustic wavefield: A new paradigm in studying geophysical phenomena. *Reviews of Geophysics*, *48*(4), 1-23. doi: 10.1029/2010RG000335

Bedard, A. J. (1971). Seismic Response of Infrasonic Microphones. *Journal of Research of the National Bureau of Standards - C. Engineering and Instrumentation*, *75C*(1), 41–45.

Cook, R. K. (1971). Infrasound radiated during the montana earthquake of 1959 august 18. *Geophysical Journal of the Royal Astronomical Society*, *26*(1–4), 191–198. doi: 10.1111/j.1365-246X.1971.tb03393.x

Ebel, J. E., Vudler, V., & Celata, M. (1982). The 1981 microearthquake swarm near Moodus, Connecticut. *Geophysical Research Letters*, *9*(4), 397–400. doi: 10.1029/GL009i004p00397

Hill, D. P., Fischer, F. G., Lahr, K. M., & Coakley, J. M. (1976). Earthquake sounds generated by body-wave ground motion. *Bulletin of the Seismological Society of America*, *66*(4), 1159–1172.

Hillers, G., T. Vuorinen, T. A., Uski, M. R., Kortström, J. T., Mäntyniemi, P. B., Tiira, T., … Saarno, T. (2020). The 2018 Geothermal Reservoir Stimulation in Espoo/Helsinki, Southern Finland: Seismic Network Anatomy and Data Features. *Seismological Research Letters*. doi: 10.1785/0220190253

Johnson, J. B., Mikesell, T. D., Anderson, J. F., & Liberty, L. M. (2020). Mapping the sources of proximal earthquake infrasound. *Geophysical Research Letters*, *47*(23), 19. doi: 10.1029/2020GL091421

Kim, T. S., Hayward, C., & Stump. (2004). Local infrasound signals from the tokachi-oki earthquake. *Geophysical Research Letters*, *31*(20), L20605. doi: 10.1029/2004GL021178

Krischer, L., Megies, T., Barsch, R., Beyreuther, M., Lecocq, T., Caudron, C., & Wassermann, J. (2015). ObsPy: a bridge for seismology into the scientific Python ecosystem. *Computational Science & Discovery*, *8*(1), 1–17. doi: 10.1088/1749-4699/8/1/014003

Kwiatek, G., Saarno, T., Ader, T., Bluemle, F., Bohnhoff, M., Chendorain, M., … et al. (2019). Controlling fluid-induced seismicity during a 6.1-km-deep geothermal stimulation in Finland. *Science Advances*, *5*. doi: 10.1126/sciadv.aav7224

Le Pichon, A., Guilbert, J., Vallée, M., Dessa, J. X., & Ulziibat, M. (2003). Infrasonic imaging of the Kunlun Mountains for the great 2001 China earthquake. *Geophysical Research Letters*, *30*(15). doi: 10.1029/2003GL017581

Le Pichon, A., Mialle, P., Guilbert, J., & Vergoz, J. (2006). Multistation infrasonic observations of the Chilean earthquake of 2005 June 13. *Geophysical Journal International*, *167*(2), 838-844. doi: 10.1111/j.1365-246X.2006.03190.x

Marcillo, O., Johnson, J. B., & Hart, D. (2012). Implementation, characterization, and evaluation of an inexpensive low-power low-noise infrasound sensor based on a micromachined differential pressure transducer and a mechanical filter. *Journal of Atmospheric and Oceanic Technology*, *29*(9), 1275–1284. doi: 10.1175/JTECH-D-11-00101.1

Michael, A. J. (2019). Earthquake Sounds. In H. K. Gupta (Ed.), *Encyclopedia of solid earth geophysics* (p. 1–5). Springer International Publishing. doi: 10

.1007/978-3-030-10475-7_201-1

Mikumo, T. (1968). Atmospheric pressure waves and tectonic deformation associated with the Alaskan earthquake of March 28, 1964. *Journal of Geophysical Research*, *73*(6), 2009–2025. doi: 10.1029/JB073i006p02009

Mutschlecner, J. P., & Whitaker, R. W. (2005). Infrasound from earthquakes. *Journal of Geophysical Research*, *110*(1), 1–11. doi: 10.1029/2004JD005067

Olson, J. V., Wilson, C. R., & Hansen, R. A. (2003). Infrasound associated with the 2002 Denali fault earthquake, Alaska. *Geophysical Research Letters*, *30*(23). doi: 10.1029/2003GL018568

Shani-Kadmiel, S., Assink, J. D., Smets, P. S. M., & Evers, L. G. (2018). Seismoacoustic Coupled Signals From Earthquakes in Central Italy: Epicentral and Secondary Sources of Infrasound. *Geophysical Research Letters*, *45*(1), 427–435. doi: 10.1002/2017GL076125

Sylvander, M., & Mogos, D. G. (2005). The sounds of small earthquakes: Quantitative results from a study of regional macroseismic bulletins. *Bulletin of the Seismological Society of America*, *95*(4), 1510–1515. doi: 10.1785/0120040197

Sylvander, M., Ponsolles, C., Benahmed, S., & Fels, J. F. (2007). Seismoacoustic recordings of small earthquakes in the Pyrenees: Experimental results. *Bulletin of the Seismological Society of America*, *97*(1 B), 294-304. doi: 10.1785/0120060009

Thouvenot, F., Jenatton, L., & Gratier, J.-P. (2009). 200-m-deep earthquake swarm in Tricastin (lower Rhône Valley, France) accounts for noisy seismicity over past centuries. *Terra Nova*, *21*(3), 203–210. doi: 10.1111/j.1365-3121.2009.00875.x

Young, J., & Greene, G. (1982). Anomalous infrasound generated by the Alaskan earthquake of 28 March 1964. *The Journal of the Acoustical Society of America*, *71*, 334–339. doi: 10.1121/1.387457